High-Frame-Rate Projection with Thousands of Frames Per Second Based on the Multi-Bit Superimposition Method

Soran Nakagawa*
Tokyo Institute of Technology

Yoshihiro Watanabe†
Tokyo Institute of Technology

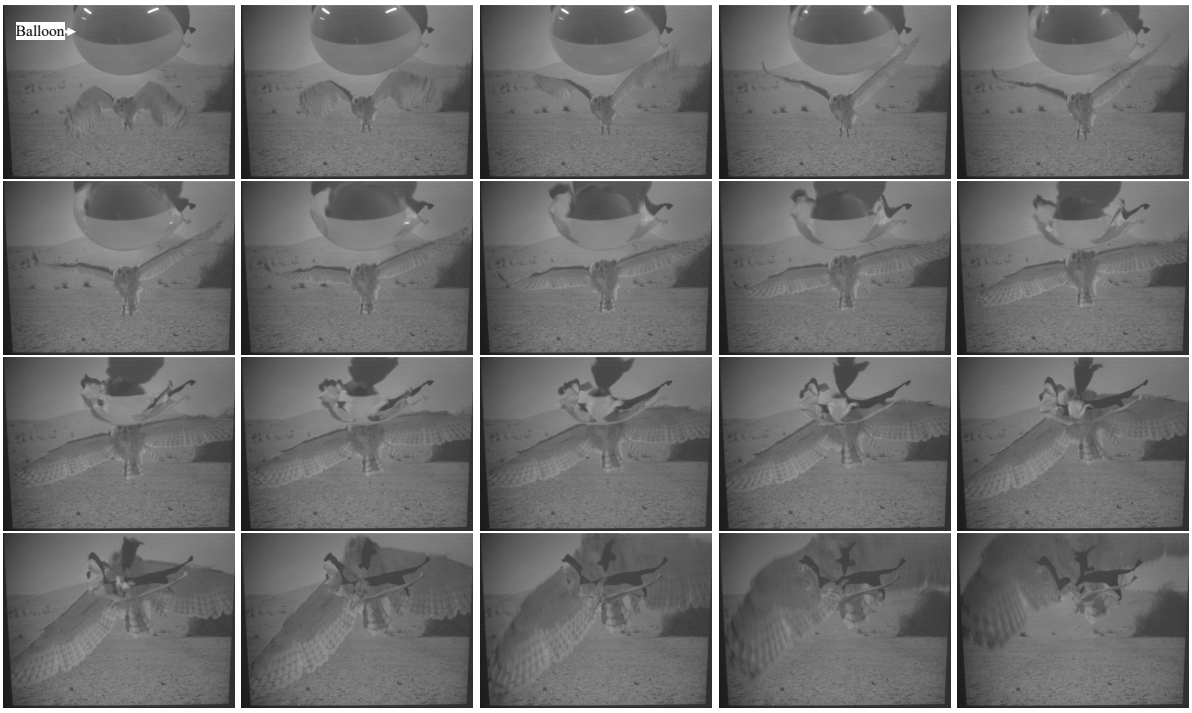

Figure 1: 5,600-fps 8-bit projection with balloon bursting. The shown images were captured at 5,600 fps in synchronization.

Abstract

The growing need for high-frame-rate projectors in the fields of dynamic projection mapping (DPM) and three-dimensional (3D) displays has increased. Conventional methods allow for an increase in the frame rate to as much as 2,841 frames per second (fps) for 8-bit image projection, using digital light processing (DLP) technology when the minimum digital mirror device (DMD) control time is 44 μs. However, this rate needs to be further augmented to suit specific applications. In this study, we developed a novel high-frame-rate projection method, which divides the bit depth of an image among multiple projectors and simultaneously projects them in synchronization. The simultaneously projected bit images are superimposed such that a high-bit-depth image is generated within a reduced single-frame duration. Additionally, we devised an optimization process to determine the system parameters necessary for attaining maximum brightness. We constructed a prototype system utilizing two high-frame-rate projectors and validated the feasibility of using our system to project 8-bit images at a rate of 5,600 fps. Furthermore, the quality assessment of our projected image exhibited superior performance in comparison to a dithered image.

*e-mail: nakagawa.s.ak@m.titech.ac.jp
†e-mail: watanabe.y.cl@m.titech.ac.jp

Index Terms: Human-centered computing—Human computer interaction (HCI)—Interaction paradigms—Mixed / augmented reality; Hardware—Communication hardware, interfaces, and storage—Displays and imagers

1 Introduction

Projectors play an essential role in various display applications, ranging from expansive video presentations to augmented reality, and are pivotal in computer vision to facilitate numerous measurements. Over time, the attributes of projectors, such as resolution, brightness, color fidelity, and frame rate, have advanced to meet diverse requirements. This study specifically focused on the aspect of frame rate, as conventional standards typically range from 30 to 60 frames per second (fps). However, the requirement to elevate the frame rate to thousands of fps to explore innovative applications has been recently identified.

For example, in the gaming domain, enhancing the frame rate to minimize latency between user input and display, and to render fluid animations, is critical to fully harness a user's capabilities [11,31,40]. Therefore, the frame rate of gaming monitors is consistently enhanced, with the latest models achieving up to 500 fps [1]. However, this upgrade is anticipated to be an ongoing process, with further amplification in frame rate required to determine the perceptual threshold beyond which further increases become imperceptible.

Similarly, dynamic projection mapping (DPM) necessitates high frame rates to mitigate misalignment between mobile targets and projected images [5, 16, 18, 33, 36]. To render such misalignment

undetectable, the latency from target movement to projection completion must be less than several milliseconds [34, 37]. Within this timeframe, DPM must execute image capture, target identification, graphics rendering, image transmission, and projection. If one hypothesizes a scenario in which the implementation consists of five segmented subtasks in a pipeline operation with a latency of 5 ms, the frame rate must be at least 1,000 fps to ensure all projection tasks are accomplished within this 5 ms window. As target recognition and rendering grow more complex and thus necessitate more pipelined subtasks to maintain high throughput and low latency, and as the perceivable latency is further reduced based on the application and observational context, a significantly higher frame rate will be required in the future.

Three-dimensional (3D) displays, including swept-volume [14, 44] and time-multiplexing light-field displays [12, 22, 42, 43, 50, 52], also necessitate a high frame rate. These displays comprise a high-frame-rate projector in conjunction with a spinning screen, where the pattern projected onto the screen manifests as a 3D image. Notable advantages of these 3D displays include a broad viewing angle and a glass-free solution that avoids accommodation–convergence conflicts.

Nevertheless, the employment of these displays inevitably requires a high-frame-rate projector operating around 5,000 fps. To meet these specifications, the bit depth of a projected image in each color channel is traditionally restricted to one or two bits. Even though dithering techniques were implemented to offset this bit-depth reduction [4, 15, 17, 45], the resultant image quality did not adequately replicate intricate texture structures on 3D surfaces. Efforts to overcome this quality degradation in swept-volume display through the use of screens with physical materials have been documented [3]; however, this approach limits the variability in displayed content. In essence, a straightforward and efficacious solution for these 3D displays lies in the realization of a projector capable of both high frame rates and high bit depths. Such performance enhancements will also be beneficial for other time-multiplexed 3D displays such as tomographic displays [10,21] and computer-generated holography [9, 13].

Furthermore, an increase in frame rate can augment the depth of the field [8, 27, 38, 51]. This method enables a fast-tunable lens to rapidly modulate the focal length, project multiple images in harmony, and attain an all-in-focus projection over an extensive depth. Such an extended depth-of-field is promising for applications, such as near-eye displays, DPM, and 3D swept-volume displays due to the broad fluctuations in target depth. The required frame rate is the product of the number of projected images in a given period and the oscillation rate; consequently, the oscillation rate must be the same as the refresh rate demanded in each specific application where the refresh rate is already elevated.

While conventional projection relies on three primary colors, increasing the number of primary colors serves to expand the gamut, facilitate projection onto non-white surfaces, and reproduce high-fidelity spectral images. The development of spectral projection with six primary colors has demonstrated its significance [20, 25]. If the projection relies on a time-multiplexing principle, such as digital light processing (DLP), a higher frame rate will facilitate the achievement of a greater number of primary colors, as all colors must be projected within a single frame time. This technique is particularly beneficial when combined with DPM that operates with a frame time of less than 1 ms.

The projector–camera configuration is crucial in enabling the acquisition of 3D shapes [53], light transport [26,35,39], and spectral reflectance [19, 28]. High-frame-rate acquisition is sought after in applications such as inspection, robotics, and scientific measurement. The most advanced high-speed cameras can record images at rates exceeding 10,000 fps [2], illustrating a substantial disparity between the frame rates achieved by cameras and those by projectors.

In this context, a high-frame-rate DLP projector capable of 8-bit image projection at 2,841 fps has been developed [30, 48, 49]. This advanced projector has already proven instrumental in the aforementioned innovative applications [8, 18, 32, 46]. Nevertheless, as previously noted, a significantly higher frame rate with a projection depth of at least 8 bits is anticipated to broaden potential applications.

The current study introduces a method for high-frame-rate projection, accommodating thousands of frames per second. Traditional DLP projectors sequentially project each bit. We partition the bit depth of the image across multiple projectors and orchestrate their simultaneous projection. The individual bit images projected in this manner are superimposed, allowing the frame rate to be amplified by adjusting the number of divisions. Furthermore, we proffer an optimization method to ascertain the division scheme, digital mirror device (DMD) control time, and light modulation tailored to the specific number of projectors and target frame rates, all aiming to maximize brightness. By developing a system with two projectors, we demonstrate that our system can achieve 5,600 fps with 8-bit image projection.

2 Related Work

2.1 High-Speed Projection

Recent digital projectors can be categorized based on their liquid-crystal, laser-scanning, and DMD configurations. Among these, DMD-type projectors excel in terms of frame rate. In such projectors, small mirrors are arrayed in accordance with the number of resolutions. Each mirror can be tilted at two different angles. At one angle, the light reflected onto the mirror is emitted through the lens; at the alternative angle, the light is not transmitted, allowing for the manipulation of the projected image. In the projected image, the brightness of each pixel is modulated by the flipping of mirrors. The frame rate, contingent on DMD control, is constrained by the employed devices. If the minimum time for DMD control is denoted by $\widetilde{T}$, the maximum frame rate for 8-bit projection becomes $\frac{1}{255\widetilde{T}}$, since the least significant bit (LSB) cannot be shorter than $\widetilde{T}$.

To overcome this limitation in color projection, 3-chip-DLP configurations, which mount three DMDs in a projector, are typically used. In this setup, the images for red, green, and blue channels are projected simultaneously, rendering the frame rate three times faster compared to a single-chip-DLP configuration with only one DMD. This method enhances the brightness, yet the increase in frame rate is limited to a factor of three for color projection in a 3-chip-DLP configuration. Although our study draws inspiration from this setup, we refined it further by dividing the image at the bit level to enhance the frame rate. The proposed method can be employed in conjunction with the 3-chip-DLP approach.

The next technique overcomes the constraints of DMD control time in single-chip configurations by introducing a synchronized high-speed light-source blinking control. Assuming the utilization of a high-speed modulatable light source such as an LED, the minimum time for the LSB in the image can be considerably reduced compared to the time restricted by the DMD, thus maximizing the frame rate for 8-bit projection to $\frac{1}{8\widetilde{T}}$. A diagram detailing the timing at this maximal frame rate is provided in Fig. 2. Therefore, this approach is anticipated to attain a frame rate approximately 32 times ($\frac{255}{8} \simeq 32$) higher than that of conventional DLP projection. A detailed exposition of this scheme follows in the next section.

Though the foundational concept was proposed in 2008 [6], the realization of an actual high-frame-rate projector was reported in 2015 [49]. This technology accomplished 1,000-fps 8-bit projection at a resolution of $1,024 \times 768$, with the delay from image generation to projection confined within 3 ms. A similar configuration was employed in 2016 to create a high-bit-depth projector [7], and in 2019, a 947-fps 24-bit projector with a resolution of $1,024 \times 768$ and

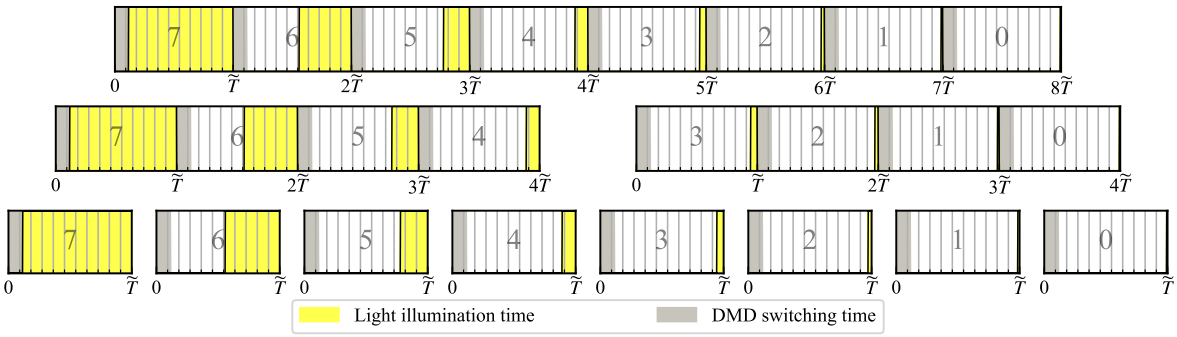

Figure 2: Comparative analysis of single-frame projection between the conventional high-frame-rate projector (top) and our proposed methodology (middle and bottom). The introduced method significantly reduces the required projection time in contrast to a conventional projector. Sequentially from top to bottom, the number of projectors N_p is specified as 1, 2, and 8, respectively.

a 2 ms delay was reported [48]. This corresponds to an achievable frame rate of 2,841 fps for 8-bit image projection, where $\widetilde{T}$ in the utilized DMD was 44 μs. Utilizing this high-frame-rate projection methodology, our study realized a substantially elevated frame rate.

Moreover, specialized high-frame-rate projectors have been devised to correct the misalignment in dynamic projection mapping [23,24] and for optical-see-through head-mounted displays [29]. These methods project binary images, with each image being warped to rectify the misalignment between the target and the projected image. Although this technique offers notable benefits, its objective diverges from the goal of the present study: the realization of high-frame-rate projection with multi-bit depth for diverse applications.

2.2 Dithering

In DLP, the frame rate can be increased by reducing the bit depth. Dithering is a prevalent technique to mitigate this decrease in bit depth, thereby generating low-bit-depth images that the human eye perceives as high-bit-depth images.

Dithering entails the conversion of an image into a lower bit-depth version—for instance, from an 8-bit image to a binary one—through various thresholding techniques. Random dithering applies a random threshold to each pixel [17], although this leads to a loss of the original image's details.

In contrast, ordered dithering employs a matrix containing thresholds. The image is divided into blocks corresponding in size to the matrix and then converted according to the matrix's thresholds. Different matrices yield various patterns: the matrix by the Bayer method results in a cross-hatch pattern [4], while the matrix by the void-and-cluster method produces blue noise [45]. Specialized ordered dithering methods for time-multiplexed light-field displays have also been developed [41].

Error-diffusion dithering can better preserve the original image's details compared to the aforementioned techniques. This method diffuses the quantization error between the original and dithered values to adjacent pixels. The Floyd-Steinberg method, based on this approach, is widely employed [15].

Nonetheless, it remains difficult for dithered images to flawlessly retain the details of high spatial frequency and smooth shading features found in the original image. Artifacts can be easily observed when the viewer looks closer to a dithered image. Additionally, since high-frame-rate projectors tend to have low spatial resolution, artifacts are rarely hidden in such situations. Our proposed approach offers a promising alternative for high-frame-rate projections across a broad spectrum of applications that do not rely on dithering.

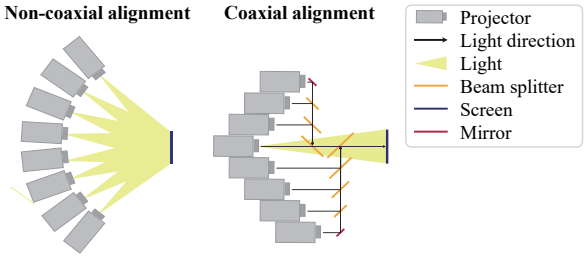

Figure 3: Illustrations of projector alignment for the multi-bit superimposing method utilizing eight projectors ($N_p = 8$). The left side depicts non-coaxial alignment, whereas the right side represents coaxial alignment.

3 Multi-bit Superimposing Projection

3.1 Overview

Our approach relies on a DLP scheme wherein the projected image is governed by the DMD and the light source. In this arrangement, an image is segmented into binary images at each bit level and then projected in sequence. Moreover, our method is founded on the technique of augmenting the frame rate, as elucidated in Sect. 2.1, where light intensity is modulated in synchrony with DMD flipping. The timing diagram for 8-bit image projection, with $\widetilde{T}$ denoting the minimum time necessary for DMD control, is illustrated at the top of Fig. 2. In this figure, eight blocks of 8 bits are shown, with yellow indicating the periods during which light is illuminated in each block. Gray designates the DMD switching period, when illumination must be withheld.

To achieve elevated frame rates, the proposed method deploys multiple projectors, synchronized with high precision. The images projected by these devices are aligned to create a single coherent image. Multiple projectors can be situated side by side, with image warping as depicted on the left side of Fig. 3, or coaxially aligned with optical elements to modify light paths, as shown on the right side of Fig. 3. The selection of alignment depends on the specifications of the utilized projectors, as non-coaxial and coaxial alignments present challenges related to focus and energy loss, respectively.

Utilizing the bit-temporally-sequential projection method described above, the binary bit images are divided into groups and assigned to different projectors. These projectors concurrently project their allocated bit images. The bit images projected simultaneously by the different projectors are superimposed and those projected sequentially by a single projector integrate into our vision. This

process allows us to substantially reduce the frame time, thereby increasing the frame rate, all while preserving high-bit-depth projection.

An illustration of the timing diagram in a two-projector configuration for 8-bit image projection is shown in the middle of Fig. 2. Here, the upper 4-bit images are projected by one projector, and the lower 4-bit images by the other. If the minimum time required for DMD control, $\widetilde{T}$, is 44 μs, the resulting frame rate is 5,682 fps, with a frame time of 176 μs. A timing diagram for an 8-projector configuration is shown at the bottom of Fig. 2. The frame rate with the 8-bit image projection and $\widetilde{T}$ =44 μs is 22,727 fps. Notably, the maximum frame rate for binary projection in the conventional scheme with $\widetilde{T}$ =44 μs is also 22,727 fps.

In summary, let N_p represent the number of projectors, and N_b denote the bit depths. Our method allows for a single projector to project up to $k = \lceil \frac{N_b}{N_p} \rceil$ bits of images, without separating a single-bit image across multiple projectors. Therefore, the frame time when employing our method can be reduced by a factor of $\frac{N_b}{k}$, compared to a conventional high-frame-rate projector.

3.2 Bit-Sequence Optimization

This section describes the optimization method used to determine the bit sequence. The method aims to minimize light loss through careful adjustment of the bit allocation to the projectors, control time of the DMD, and light illumination time. Specifically, in the optically coaxial configuration, each projector might be equipped with a beam splitter to combine its light with others, as depicted on the right side of Fig. 3. Further, our method can be used to determine the optimal characteristics of such optical components. This optimization is designed on the basis of mixed-integer nonlinear programming (MINLP), and the optimization parameters are as follows:

$N_p \in \mathbb{N}$	:	Number of projectors
$N_b \in \mathbb{N}$	:	Number of bits of projected image
$\dot{T}$	:	Time consumed by a single frame projection
$\widetilde{T}$	:	Minimum time of DMD control
$\widehat{T}$	:	Minimum time of light-off to avoid projection while DMD switching

The optimized parameters are as follows:

$\boldsymbol{\xi} \in \mathbb{R}^{N_p}$ $[\xi_0, \ldots, \xi_{N_p-1}]^T$	:	Attenuation rate per projector
$\boldsymbol{H} \in \{0,1\}^{N_p \times N_b}$	:	Bit allocation status
$\widetilde{\boldsymbol{t}} \in \mathbb{R}^{N_b}$ $[\widetilde{t}_0, \ldots, \widetilde{t}_{N_b-1}]^T$	:	DMD control time for each bit
$\widehat{\boldsymbol{t}} \in \mathbb{R}^{N_b}$ $[\widehat{t}_0, \ldots, \widehat{t}_{N_b-1}]^T$	:	Illumination time for each bit

The vector $\boldsymbol{\xi}$ is applied in the context of optical coaxial alignment. If the available beam splitter is predetermined, $\boldsymbol{\xi}$ can be considered a given parameter. Conversely, when coaxial alignment is not employed, and the projectors are arrayed side-by-side, as shown on the left side of Fig. 3, $\boldsymbol{\xi}$ also becomes a given parameter, with all its values set to one. $H_{i,j}$ in $\boldsymbol{H}$ is the j-th bit's allocation status for the ith projector. If $H_{i,j}$ equals 1, the j-th bit is assigned to projection by the ith projector. $\widetilde{t}_i$ and $\widehat{t}_i$ are the DMD control and illumination times for the i-th bit, respectively.

With these parameters, the optimization aims to enhance the brightness of the system. The goal function to be maximized, along with the associated constraints, are as follows:

$$
\begin{aligned}
\underset{\boldsymbol{\xi},\boldsymbol{H},\widetilde{\boldsymbol{t}},\widehat{\boldsymbol{t}}}{\text{maximize}} \quad & f(\boldsymbol{\xi},\boldsymbol{H},\widehat{\boldsymbol{t}}) = \boldsymbol{\xi}^T \cdot \boldsymbol{H} \cdot \widehat{\boldsymbol{t}} \\
\text{subject to} \quad & \\
& \widetilde{t}_i \geq \widetilde{T} && \forall i \in [0, N_b) \\
& \widetilde{t}_i \geq \widehat{t}_i + \widehat{T} && \forall i \in [0, N_b) \\
& (\boldsymbol{\xi}^T \cdot \boldsymbol{H})_{i+1} \cdot \widehat{t}_{i+1} = (\boldsymbol{\xi}^T \cdot \boldsymbol{H})_i \cdot \widehat{t}_i \cdot 2 && \forall i \in [0, N_b - 1) \\
& (\boldsymbol{H} \cdot \widetilde{\boldsymbol{t}})_p \leq \dot{T} && \forall p \in [0, N_p) \\
& (\boldsymbol{H}^T \cdot \boldsymbol{H})_{i,i} = 1 && \forall i \in [0, N_b) \\
& ||\boldsymbol{\xi}||_1 = 1 && \text{for coaxial case}
\end{aligned}
$$

The objective function $f(\boldsymbol{\xi},\boldsymbol{H},\widehat{\boldsymbol{t}})$ represents the brightness achieved by the projection system. The control time of the DMD for each bit must exceed $\widetilde{T}$, as demonstrated in the first constraint, due to the intrinsic device limitations of the DMD. Within the bounds of the DMD's control time, the illumination time for each bit is modulated to be appreciably extended, as specified by the second constraint. The system is obliged to satisfy the third constraint, which ensures that the brightness of each bit augments by a factor of 2. The control time of the DMD is restricted by the frame time, as expressed in the fourth constraint. According to the fifth constraint, each bit must be allocated to a projector. The sixth constraint is invoked when the optical axes of the projectors are aligned, and it governs the optimization of the attenuation rates per projector. The constraint $\xi_i \geq 0$ $(\forall i \in [0, N_p))$ is omitted as it is considered redundant.

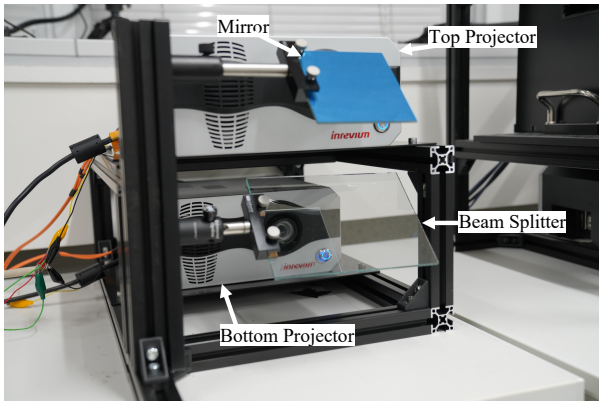

Figure 4: Schematic of our experimental projection system employing two projectors. The illumination from the upper projector undergoes reflection by the mirror and is subsequently combined with the light from the lower projector via the beam splitter (R/T = 30/70).

4 Developed System with Two Projectors

4.1 System Configuration

An illustration of the constructed system for 8-bit image projection utilizing two projectors ($N_b = 8, N_p = 2$) is provided in Fig. 4. This arrangement employed a high-frame-rate 8-bit projector with a resolution of 1024×768 (manufactured by Tokyo Electron Device Limited, TB-UK-DYNAFLASH). The projector's frame rate was augmented in accordance with the approach described in Sect. 2.1, having parameters with $\widetilde{T} = 44$ μs and $\widehat{T} = 5$ μs. The images emitted from both projectors were aligned coaxially. For precise optical alignment, a mirror and beam splitter were positioned in front of

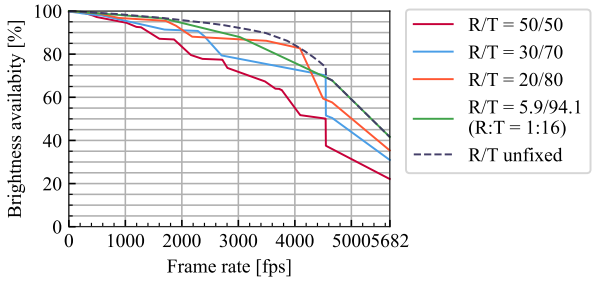

Figure 5: Examination of brightness availability dependent on the frame rate for various R/T ratios, inclusive of the scenario with an unfixed R/T rate.

the top and bottom projectors, respectively, as depicted in Fig. 4. Additional image warping was applied to achieve exact alignment[1].

4.2 Brightness Simulation

Simulations were conducted by applying our optimization computation to elucidate the effect of the refraction/transmittance (R/T) rate on the brightness of the projected images. Specifically, the brightness levels of these images were simulated, and the brightness availability across different frame rates for each fixed R/T rate was investigated. The anticipated brightness of the projected images was computed employing the objective function relevant to the optimization problem, as explicated in Sect. 3.2. Within this simulation, the R/T rate corresponds to the attenuation rate $\boldsymbol{\xi}$. The Couenne solver, in conjunction with AMPL, was utilized to effectuate our methodology. Brightness availability was defined as the ratio of our system's brightness to the theoretical brightness in a system where light intensity is governed solely by DMD, devoid of light modulation, and without light loss.

The relationship between brightness availability and frame rate for each R/T rate is shown in Fig. 5. In this figure, the horizontal and vertical axes symbolize the frame rate and brightness availability, respectively. Moreover, the figure encompasses the outcomes when the R/T rate is unfixed and considered as an estimated parameter in the optimization.

As shown in Fig. 5, various non-constant gradients are evident. A majority of these cases result from alterations in the bit allocation status $\boldsymbol{H}$. For instance, a significant decrease in brightness availability was perceived across all R/T rate cases at approximately 4,500 fps on the horizontal axis. In the instance of an unfixed R/T rate at 4,500 fps, the optimal parameters are as follows:

- $\boldsymbol{H} = \begin{bmatrix} 1 & 1 & 1 & 1 & 1 & 0 & 0 & 0 \\ 0 & 0 & 0 & 0 & 0 & 1 & 1 & 1 \end{bmatrix}$
- $\widetilde{\boldsymbol{t}}[\mu\mathrm{s}] = \begin{bmatrix} 44 & 44 & 44 & 44 & 46.22 & 44 & 61.07 & 117.15 \end{bmatrix}^T$
- $\widehat{\boldsymbol{t}}[\mu\mathrm{s}] = \begin{bmatrix} 2.58 & 5.15 & 10.31 & 20.61 & 41.22 & 28.04 & 56.07 & 112.15 \end{bmatrix}^T$
- $\boldsymbol{\xi} = \begin{bmatrix} 0.2538 & 0.7462 \end{bmatrix}^T$

The optimal bit allocation scheme deployed five bits for one projector and three bits for the other. The brightness availability was considerably diminished at approximately 4545.45 fps because this specific frame rate represented the threshold beyond which it became unfeasible to allocate five bits to a single projector ($\frac{1}{5\hat{T}} \approx 4545.45$ fps) [2].

It is important to note that for frame rates surpassing the threshold of 4545.45 fps, the bit allocation status $\boldsymbol{H}$ remains constant. Specifically, one projector is allotted the four most significant bits, while the other projector is allotted the four least significant bits, as symbolized by the matrix $\boldsymbol{H} = \begin{bmatrix} 1 & 1 & 1 & 1 & 0 & 0 & 0 & 0 \\ 0 & 0 & 0 & 0 & 1 & 1 & 1 & 1 \end{bmatrix}$ (the reverse $\boldsymbol{H} = \begin{bmatrix} 0 & 0 & 0 & 0 & 1 & 1 & 1 & 1 \\ 1 & 1 & 1 & 1 & 0 & 0 & 0 & 0 \end{bmatrix}$ is also true). Furthermore, in this case, the optimal attenuation rate of each projector (R/T ratio of the beam splitter) is expressed as $\boldsymbol{\xi} = \frac{1}{17}\begin{bmatrix} 1 & 16 \end{bmatrix}^T$ (or $\boldsymbol{\xi} = \frac{1}{17}\begin{bmatrix} 16 & 1 \end{bmatrix}^T$). In this configuration, both projectors were synchronized, possessing identical illumination and control times corresponding to the DMD. In the next section, we introduce the empirical parameters utilized in the experiments.

4.3 Optimized Parameters for the Experiments

Based on the constructed system, we fine-tuned the parameters to actualize a frame time of $\hat{T} = 177.93$ μs. We deliberately circumvented customization of the beam splitter. Based on the data depicted in Fig. 5, we incorporated a beam splitter with an R/T rate of 30/70 from readily available products. The vector $\boldsymbol{\xi}$ was fixed at $\begin{bmatrix} 0.3 & 0.7 \end{bmatrix}^T$. As a consequence, 30 % of the light from the top projector and 70 % from the bottom projector coalesced to form a unified projected image. The light blue solid line in Fig. 5 indicates the change in brightness availability when the beam splitter ratio was fixed at 30/70.

Under these specific conditions, the optimization techniques detailed in Sect. 3.2 determines the remaining parameters as follows:

- $\boldsymbol{H} = \begin{bmatrix} 1 & 1 & 1 & 1 & 0 & 0 & 0 & 0 \\ 0 & 0 & 0 & 0 & 1 & 1 & 1 & 1 \end{bmatrix}$
- $\widetilde{\boldsymbol{t}}[\mu\mathrm{s}] = \begin{bmatrix} 44 & 44 & 44 & 44 & 44 & 44 & 44 & 45.93 \end{bmatrix}^T$
- $\widehat{\boldsymbol{t}}[\mu\mathrm{s}] = \begin{bmatrix} 0.73 & 1.48 & 2.97 & 5.96 & 5.11 & 10.23 & 20.46 & 40.93 \end{bmatrix}^T$

Thus, we anticipated achieving a brightness approximately 32 % of the theoretical maximum brightness, as illustrated in Fig. 5.

5 Evaluation

5.1 Synchronized Bit Sequence

The projection of the bit sequence was assessed using Si PiN photodiodes (Hamamatsu Photonics, S5973), coupled with photosensor amplifiers (Hamamatsu Photonics, C8366). Each photodiode was positioned in alignment with the respective projector, and the outputs were gauged using an oscilloscope (Tektronix, MDO3034). The results are depicted in the upper two figures of Fig. 6. For this evaluation, an image comprising 255-pixel values was projected in accordance with the parameters defined in Sect. 4.3. The figure also illustrates the anticipated output responses in green, and the illumination pattern transpired as expected, as evidenced in Fig. 6.

Synchronization of the two projectors is imperative. To fulfill this prerequisite, each projector can be regulated to initiate the projection of a singular frame at the moment of the rising edge of the trigger signal. The response of the projectors to this trigger signal was examined, as shown in Fig. 6. A singular trigger signal was supplied to

[1] Supplementary material provides comprehensive details to replicate our system.

[2] The Supplementary material provides more comprehensive examples concerning the nonlinearity depicted in Fig. 5. Additionally, this material includes supplementary simulation results for a system encompassing three projectors.

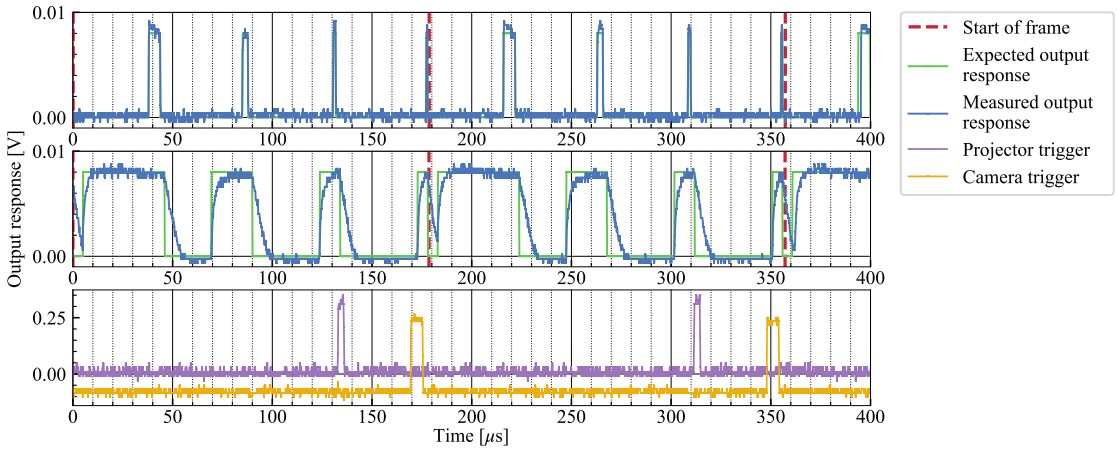

Figure 6: Display of actual and anticipated photodiode responses in the 1st and 2nd projectors, exhibited in the top and middle, respectively. Following the arrangement described in Sect. 4.3, the 1st projector is allocated the least significant four bits and identified as the top projector, while the 2nd projector is assigned the most significant four bits and recognized as the bottom projector. The bottom section illustrates the trigger signals for both projectors and the camera.

both projectors for preliminary assessment, as indicated at the lower part of Fig. 6. The red dashed lines in the top two figures demarcate the commencement time of the projection for each individual frame. Based on these findings, the variance in the start times between the two projectors was approximately 0.1 μs, a discrepancy deemed insignificant. Consequently, synchronization of the two projectors can be achieved with a single trigger signal, maintaining adequate precision. Furthermore, it was noted that the delay from the trigger input to the projection onset was approximately 46 μs.

Although the achievable frame rate of the projection system, according to the parameters in Sect. 4.3, was 5,620 fps ($\dot{T} = 177.93$ μs), the frame rate of each trigger was set at 5,600 fps for the evaluations. This moderated frame rate was necessitated for the stable synchronization.

5.2 Gradation

This section introduces the findings regarding the measured illuminance of the newly developed projector operating at 5,600 fps. An illuminometer (Konica Minolta, T-10MA) was employed, situated at the central point of the projected image and positioned 900 mm from the beam splitter in alignment with the lower projector. During this measurement, the pixel values within the projected image were maintained uniformly.

The results are depicted in Fig. 7 on a logarithmic scale. As our system refrains from utilizing gamma correction, the illuminance corresponding to each bit should be directly proportional to the gradation level represented in this graph. The illuminance altered linearly, as evidenced in the figure. To accomplish this result, we meticulously regulated the current of the LED in each projector beforehand to offset the individual variances between the two projectors.

5.3 5,600 Fps Projection

We assessed the projected image employing images captured by a high-speed camera, specifically Mikrotron, EoSens 1.1CXP2 (MC1166, monochrome), with the resolution adjusted to 720 × 540 pixels. The lens utilized was VS Technology, VS-25085/C, having a focal length of 25 mm, and the F-number was designated at 0.85. The camera's gain was maximized to a value of 4.0.

The initiation of camera exposure can coincide with the rising edge of the trigger signal. The latency from the rising edge of this

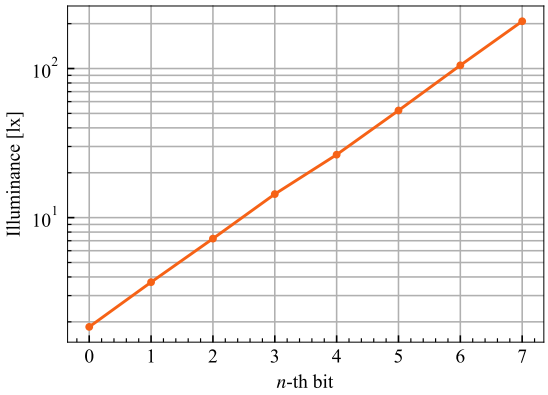

Figure 7: Illuminance on the screen of the projected images corresponding to each bit.

signal to the commencement of exposure was identified to differ from the projector's delay, which was 46 μs. Consequently, we formulated a distinct trigger signal apart from the one utilized for the projectors. Moreover, we set a period exceeding the projection frame time $\dot{T} = 177.93$ μs as noted in Sect. 5.1. As a result, we calibrated the frame rates for both projection and capturing at 5,600 fps, while keeping the projection frame time as $\dot{T} = 177.93$ μs.

Using this configuration, we manually fine-tuned the timing of the camera's trigger signal through observation of the projected image, thereby ensuring that the precise pattern was discernible in the captured images. The lower figure in Fig. 6 shows the actual timing of the trigger signal transmitted to the camera.

The distance between the system and the screen was maintained at 900 mm, as elaborated in Sect. 5.2. The camera was positioned at a distance of 1,800 mm from the screen. The results, which illustrate the capture of the 8-bit image projection at 5,600 fps, are displayed in Fig. 8. The projected image exhibited a vertically striped pattern, with values constituting $\{2^i : i = 0, 1, \ldots, 7\}$. This pattern transited from the right to the left with each frame, and the image also encompassed a counter indicating the frame number at

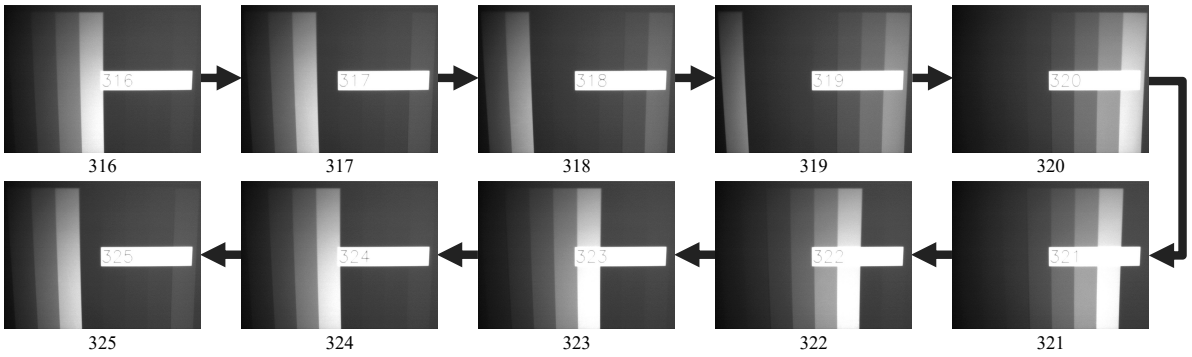

Figure 8: Images projected at 5,600 fps, depicting a vertically striped pattern that moves from right to left, inclusive of a counter denoting the frame number. The frames are captured at a rate identical to that of the projector.

the center.

As depicted in the figure, the pattern transformed with every frame, exhibiting neither repetition nor omission of frames. The images were successfully updated at a rate of 5,600 fps. Fig. 1 presents an additional projection result, captured during the bursting of a balloon to assess the speed of the phenomenon.

5.4 Image Quality

The proposed system synthesized a singular image through the deployment of two projectors. Due to this particular configuration, the potential for spatial pixel misalignment was introduced, which might consequently lead to a brightness error. This inconsistency arises when incorrect pixels from the dual projectors are superimposed as a result of the aforementioned misalignment. However, this error did not manifest in the evaluation delineated in Sect. 5.2, as all pixels maintained identical values. Therefore, this section elucidates an evaluation of image quality during the projection of a natural image.

We executed the projection of images, adhering to our proposed methodology, at a rate of 5,600 fps, and synchronously captured them. Correspondingly, we projected and captured dithered images at the same frame rate for the purpose of comparison, employing both Bayer and Floyd-Steinberg dithering techniques to convert an 8-bit reference image into a 1-bit representation. In the case of the original reference image, we projected and captured images at a rate of 60 fps. The aperture of the camera lens was manually calibrated to ensure that the mean pixel brightness within the captured images remained consistent.

The images obtained are displayed in Fig. 9. For the upper three variants within Fig. 9, the camera was positioned approximately 300 mm from the screen and was angled diagonally to avert any undesirable shadows or reflections that might be induced by the projections onto the camera. For the full image displayed in Fig. 9, the camera was stationed at a distance of approximately 1,800 mm from the screen.

A discernible difference in the gradation representation capabilities of each image is evident in the image's background (e.g., the sky). These artifacts were a consequence of the dithering method. Conversely, the image obtained through our method was corroborated to be more analogous to the original reference. Moreover, in comparison to dithering methods, our approach was able to accomplish superior quality at sharp edges (e.g., the penguins' beaks in the image).

Upon examining the texture, particularly the skin of the penguins, our method was found to clearly render the texture in a manner that more resembles natural appearance than did the dithering methods. The dithering methods revealed numerous dots within the texture, creating a visually distracting effect. In contrast, our technique provides a smoother and more harmonious portrayal of the texture, resulting in a visually appealing and realistic depiction of the penguins' skin.

For a quantitative comparison, we evaluated the image quality based on the structural similarity index (SSIM) between the reference and high-frame-rate projection images [47]. The SSIM results for the four types of images depicted in Fig. 9 are detailed in Table 1. As demonstrated in Table 1, our method surpasses the dithering methods in performance. Additionally, our approach was able to represent high-quality images irrespective of the distance between the camera and screen in this assessment.

Table 1: An evaluation of the similarity between each image and the original image (with adjusted aperture). For the similarity assessment, we utilized the SSIM.

	Bayer	Floyd-Steinberg	Our method
Gradation	0.380	0.402	**0.799**
Sharp edge	0.546	0.541	**0.754**
Texture	0.569	0.567	**0.858**
Full image	0.710	0.722	**0.798**

6 Discussion

This study introduced a system developed using two projectors with an optical coaxial alignment. Although a beam splitter with R/T = 30/70 was utilized in this study due to its availability, it is not the optimized configuration in terms of brightness, as illustrated in Fig. 5. We are obligated to illustrate the performance of the most effective system configuration.

Additionally, we did not manifest the optimal maximum frame rate projection at 5,682 fps within the developed system. This limitation arose due to two reasons. The first reason is the inability to capture satisfactory images for evaluation at the maximum frame rate, which is attributable to the low brightness of the projection. To overcome this obstacle, it is incumbent upon us to enhance the aforementioned brightness and secure a camera with higher sensitivity. The second reason, as described in Sect. 5.1, is the difficulty in achieving stable synchronization in two projectors when the trigger period and frame time are the same. We needed to set the trigger period slightly longer than the frame time due to the synchronization specification in the used projector. To surmount this obstacle, we need to improve the control circuit related to the synchronization in the projector.

The light modulation response was presumed to be a square wave; however, the factual response in the lower projector did not align with the ideal, as depicted in Fig. 6. Since the response of the upper projector was superior to that of the bottom one, this discrepancy

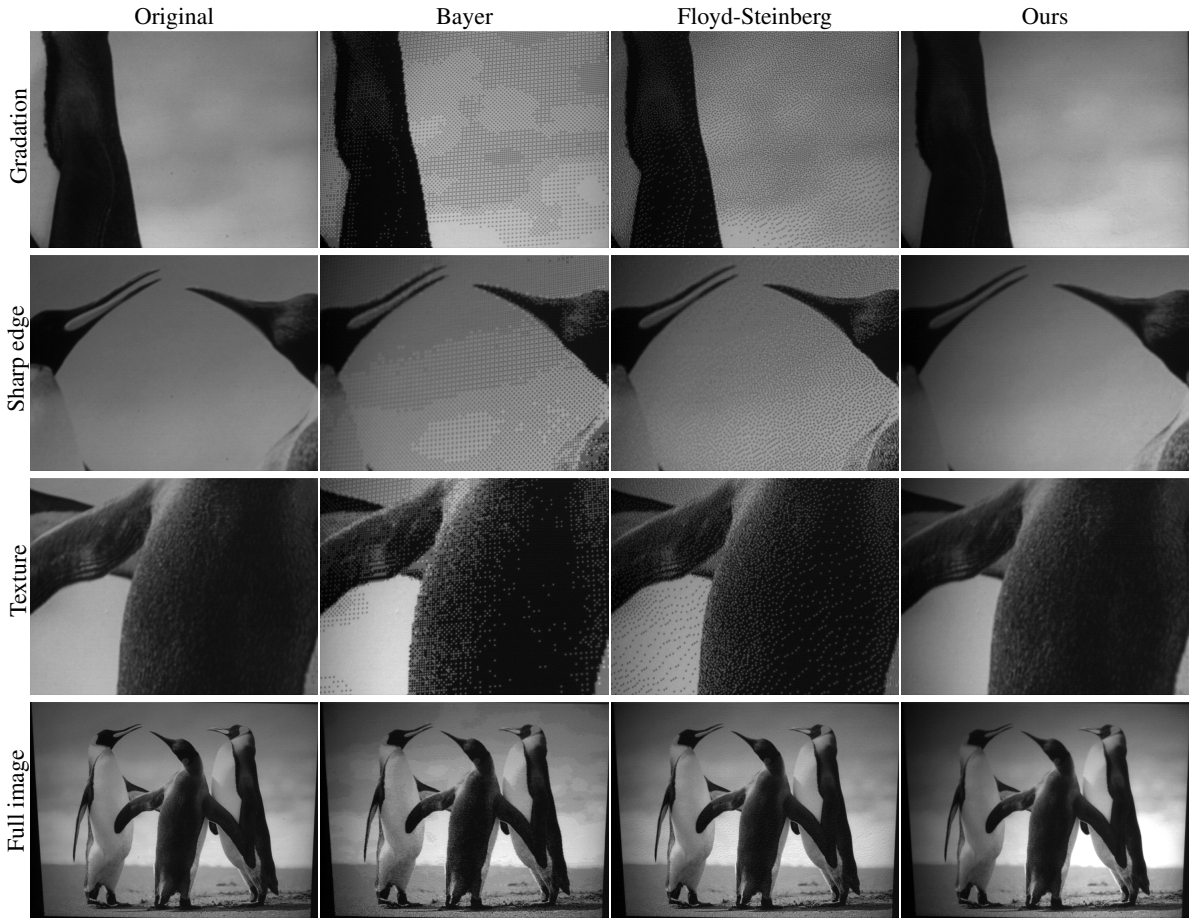

Figure 9: Comparison of various projection methods. The images, arranged from left to right, display the results of the original image (captured and projected at 60 fps), Bayer Dithering, Floyd-Steinberg Dithering, and our specific method. The results pertaining to the dithering and our methods were captured and projected at 5,600 fps. The illustrations, from top to bottom, reveal both zoomed and full images to accentuate the quality distinctions among the methods.

was not deduced to stem from the performance of the photodiode and oscilloscope. At present, this may induce a minor error margin that is perceptible in the transition from the third to the fourth bit in Fig. 7, and it may consequently diminish the image quality.

An alternative approach to augmenting the image quality would be to meticulously examine the pixel alignment precision. While the findings of this study did not reveal pronounced errors, we detected inconspicuous artifacts in the image projected by our system when juxtaposed with the original image. This discrepancy might be ascribed to image warping for coaxial alignment and bit-depth separation. As these procedures are executed independently, errors in either or both processes might engender unforeseen artifacts. We require more precise calibration and a novel method to simultaneously optimize image warping and bit sequence, particularly when implementing a higher-resolution projector or a greater quantity of projectors.

In the present study, we utilized the SSIM as our criterion for evaluating image quality. Nevertheless, it is vital to acknowledge that SSIM, similar to all other metrics, is not without its shortcomings in capturing the nuances of image quality. We acknowledge the need to further explore image quality assessments through user studies.

Furthermore, this innovation holds the potential for advancement through the employment of an increased number of projectors to attain a superior frame rate. Exploration of color projections using this methodology should also be undertaken. Moreover, beyond merely amplifying the frame rate, our projection technique is anticipated to augment the bit-depth in projections with reduced frame rates.

7 Conclusion

We introduced a multi-bit superimposition method with the aim of materializing high-speed DLP projection capable of thousands of frame rates, all the while preserving elevated bit depths. Theoretically, the proposed method can facilitate eight-fold accelerated 8-bit image projection in comparison to a solitary projector, under ideal conditions. We also elucidated an optimization procedure to ascertain the system parameters essential for optimizing the brightness of the projection.

Based on this proposal, we constructed a high-frame-rate projection system employing two projectors aligned along the same optical axis. This system was able to effectuate 8-bit projection at 5,600 fps, and, notably, could project images with a considerably higher gradation than could be achieved by a single projector using dithering at the identical frame rate.

In the future, we intend to address the challenges described in Sect. 6. Concurrently, we envision deploying the proposed projection system in the various potential applications introduced in Sect. 1.

Acknowledgments

This work was supported by JSPS KAKENHI Grant Number JP20H05959.

REFERENCES

[1] Dell Inc. AW2524H.

[2] Photron. https://photron.com/ [Accessed: 2023-06-09].

[3] R. Asahina, T. Nomoto, T. Yoshida, and Y. Watanabe. Realistic 3D swept-volume display with hidden-surface removal using physical materials. In *2021 IEEE Virtual Reality and 3D User Interfaces (VR)*, pp. 113–121, 2021. doi: 10.1109/VR50410.2021.00032

[4] B. E. Bayer. An optimum method for two-level rendition of continuous-tone pictures. *IEEE International Conference on Communications*, 1:(26–11)–(26–15), 1973.

[5] A. Bermano, M. Billeter, D. Iwai, and A. Grundhöfer. Makeup lamps: Live augmentation of human faces via projection. *Computer Graphics Forum*, 36:311–323, 2017. doi: 10.1111/cgf.13128

[6] O. Bimber, D. Iwai, G. Wetzstein, and A. Grundhöfer. The visual computing of projector-camera systems. *Computer Graphics Forum*, 27(8):2219–2245, 2008. doi: 10.1111/j.1467-8659.2008.01175.x

[7] J.-H. R. Chang, B. V. K. V. Kumar, and A. C. Sankaranarayanan. 216 shades of gray: high bit-depth projection using light intensity control. *Opt. Express*, 24(24):27937–27950, 2016. doi: 10.1364/OE.24.027937

[8] J.-H. R. Chang, B. V. K. V. Kumar, and A. C. Sankaranarayanan. Towards multifocal displays with dense focal stacks. *ACM Transactions on Graphics (TOG)*, 37(6):1–13, 2018. doi: 10.1145/3272127.3275015

[9] S. Choi, M. Gopakumar, Y. Peng, J. Kim, M. O'Toole, and G. Wetzstein. Time-multiplexed neural holography: A flexible framework for holographic near-eye displays with fast heavily-quantized spatial light modulators. In *ACM SIGGRAPH 2022 Conference Proceedings*, 2022. doi: 10.1145/3528233.3530734

[10] S. Choi, S. Lee, Y. Jo, D. Yoo, D. Kim, and B. Lee. Optimal binary representation via non-convex optimization on tomographic displays. *Opt. Express*, 27(17):24362–24381, 2019. doi: 10.1364/OE.27.024362

[11] M. Claypool, K. Claypool, and F. Damaa. The effects of frame rate and resolution on users playing first person shooter games. In *2006 ACM/SPIE Multimedia Computing and Networking*, vol. 6071. International Society for Optics and Photonics, 2006. doi: 10.1117/12.648609

[12] O. S. Cossairt, J. Napoli, S. L. Hill, R. K. Dorval, and G. E. Favalora. Occlusion-capable multiview volumetric three-dimensional display. *Appl. Opt.*, 46(8):1244–1250, 2007. doi: 10.1364/AO.46.001244

[13] V. R. Curtis, N. W. Caira, J. Xu, A. G. Sata, and N. C. Pégard. DCGH: Dynamic computer generated holography for speckle-free, high fidelity 3D displays. In *2021 IEEE Virtual Reality and 3D User Interfaces (VR)*, pp. 1–9, 2021. doi: 10.1109/VR50410.2021.00097

[14] G. E. Favalora, J. Napoli, D. M. Hall, R. K. Dorval, M. Giovinco, M. J. Richmond, and W. S. Chun. 100-million-voxel volumetric display. In *Cockpit Displays IX: Displays for Defense Applications*, vol. 4712, pp. 300–312, 2002. doi: 10.1117/12.480930

[15] R. W. Floyd and L. Steinberg. An adaptive algorithm for spatial greyscale. In *Society for Information Display*, vol. 17, pp. 75–77, 1976.

[16] K. Fukamizu, L. Miyashita, and M. Ishikawa. Elamorph projection: Deformation of 3D shape by dynamic projection mapping. In *2020 IEEE International Symposium on Mixed and Augmented Reality (ISMAR)*, pp. 164–173, 2020. doi: 10.1109/ISMAR50242.2020.00038

[17] W. M. Goodall. Television by pulse code modulation. *Bell System Technical Journal*, 30(1):33–49, 1951. doi: 10.1002/j.1538-7305.1951.tb01365.x

[18] A. Grundhöfer and D. Iwai. Recent advances in projection mapping algorithms, hardware and applications. *Computer Graphics Forum*, 37:653–675, 2018. doi: 10.1111/cgf.13387

[19] S. Han, I. Sato, T. Okabe, and Y. Sato. Fast spectral reflectance recovery using DLP projector. In *10th Asian Conference on Computer Vision*, pp. 323–335, 2011. doi: 10.1007/s11263-013-0687-z

[20] K. Hirai, D. Irie, and T. Horiuchi. Multi-primary image projector using programmable spectral light source. *Journal of the Society for Information Display*, 24(3):144–153, 2016. doi: 10.1002/jsid.422

[21] Y. Jo, S. Lee, D. Yoo, S. Choi, D. Kim, and B. Lee. Tomographic projector: Large scale volumetric display with uniform viewing experiences. *ACM Transactions on Graphics (TOG)*, 38(6), 2019. doi: 10.1145/3355089.3356577

[22] A. Jones, I. McDowall, H. Yamada, M. Bolas, and P. Debevec. Rendering for an interactive 360° light field display. *ACM Transactions on Graphics (TOG)*, 26(3):40–es, 2007. doi: 10.1145/1276377.1276427

[23] S. Kagami and K. Hashimoto. Sticky projection mapping: 450-fps tracking projection onto a moving planar surface. In *SIGGRAPH Asia 2015 Emerging Technologies*, 2015. doi: 10.1145/2818466.2818485

[24] S. Kagami and K. Hashimoto. A full-color single-chip-DLP projector with an embedded 2400-fps homography warping engine. In *ACM SIGGRAPH 2018 Emerging Technologies*, 2018. doi: 10.1145/3214907.3214927

[25] I. Kauvar, S. J. Yang, L. Shi, I. McDowall, and G. Wetzstein. Adaptive color display via perceptually-driven factored spectral projection. *ACM Transactions on Graphics (TOG)*, 34(6), 2015. doi: 10.1145/2816795.2818070

[26] H. Kubo, S. Jayasuriya, T. Iwaguchi, T. Funatomi, Y. Mukaigawa, and S. G. Narasimhan. Acquiring and characterizing plane-to-ray indirect light transport. In *2018 IEEE International Conference on Computational Photography (ICCP)*, pp. 1–10, 2018. doi: 10.1109/ICCPHOT.2018.8368461

[27] S. Lee, Y. Jo, D. Yoo, J. Cho, D. Lee, and B. Lee. Tomographic near-eye displays. *Nature Communications*, 10:2497, 2019. doi: 10.1038/s41467-019-10451-2

[28] C. Li, Y. Monno, H. Hidaka, and M. Okutomi. Pro-cam SSfM: Projector-camera system for structure and spectral reflectance from motion. In *2019 IEEE/CVF International Conference on Computer Vision (ICCV)*, pp. 2414–2423, 2019. doi: 10.1109/ICCV.2019.00250

[29] P. Lincoln, A. Blate, M. Singh, T. Whitted, A. State, A. Lastra, and H. Fuchs. From motion to photons in 80 microseconds: Towards minimal latency for virtual and augmented reality. *IEEE Transactions on Visualization and Computer Graphics*, 22(4):1367–1376, 2016. doi: 10.1109/TVCG.2016.2518038

[30] U. Lippmann, P. Aswendt, R. Hoefling, K. Sumino, K. Ueda, Y. Ono, H. Kasebe, T. Yamashita, T. Yuasa, and Y. Watanabe. High-speed RGB+IR projector based on coaxial optical design with two digital mirror devices. *International Display Workshops*, pp. 636–639, 2021. doi: 10.36463/idw.2021.0636

[31] S. Liu, A. Kuwahara, J. J. Scovell, and M. Claypool. The effects of frame rate variation on game player quality of experience. In *2023 CHI Conference on Human Factors in Computing Systems*, 2023. doi: 10.1145/3544548.3580665

[32] M. Maruyama, S. Tabata, Y. Watanabe, and M. Ishikawa. Multi-pattern embedded phase shifting using a high-speed projector for fast and accurate dynamic 3D measurement. In *2018 IEEE Winter Conference on Applications of Computer Vision (WACV)*, pp. 921–929, 2018. doi: 10.1109/WACV.2018.00106

[33] G. Narita, Y. Watanabe, and M. Ishikawa. Dynamic projection mapping onto deforming non-rigid surface using deformable dot cluster marker. *IEEE Transactions on Visualization and Computer Graphics*, 23(3):1235–1248, 2017. doi: 10.1109/TVCG.2016.2592910

[34] A. Ng, J. Lepinski, D. Wigdor, S. Sanders, and P. Dietz. Designing for low-latency direct-touch input. In *25th Annual ACM Symposium on User Interface Software and Technology*, p. 453–464, 2012. doi: 10.1145/2380116.2380174

[35] K. Nishino, A. Subpa-Asa, Y. Asano, M. Shimano, and I. Sato. Variable ring light imaging: capturing transient subsurface scattering with an ordinary camera. In *European Conference on Computer Vision (ECCV)*, pp. 598–613, 2018.

[36] T. Nomoto, W. Li, H.-L. Peng, and Y. Watanabe. Dynamic multi-projection mapping based on parallel intensity control. *IEEE Transactions on Visualization and Computer Graphics*, 28(5):2125–2134, 2022. doi: 10.1109/TVCG.2022.3150488

[37] H.-L. Peng, S. Nishida, and Y. Watanabe. Studying user perceptible misalignment in simulated dynamic facial projection mapping. In *2023 IEEE International Symposium on Mixed and Augmented Reality (ISMAR)*, 2023.

[38] K. Rathinavel, H. Wang, A. Blate, and H. Fuchs. An extended depth-at-field volumetric near-eye augmented reality display. *IEEE Transactions on Visualization and Computer Graphics*, 24(11):2857–2866, 2018. doi: 10.1109/TVCG.2018.2868570

[39] P. Sen, B. Chen, G. Garg, S. R. Marschner, M. Horowitz, M. Levoy, and H. P. A. Lensch. Dual photography. In *ACM SIGGRAPH 2005*

Papers, p. 745–755, 2005. doi: 10.1145/1186822.1073257

[40] J. Spjut, B. Boudaoud, K. Binaee, J. Kim, A. Majercik, M. McGuire, D. Luebke, and J. Kim. Latency of 30 ms benefits first person targeting tasks more than refresh rate above 60 Hz. In *SIGGRAPH Asia 2019 Technical Briefs*, p. 110–113, 2019. doi: 10.1145/3355088.3365170

[41] C. Su, Q. Zhong, Y. Peng, L. Xu, R. Wang, H. Li, and X. Liu. Grayscale performance enhancement for time-multiplexing light field rendering. *Opt. Express*, 23(25):32622–32632, 2015. doi: 10.1364/OE.23.032622

[42] C. Su, X. Zhou, H. Li, Q. Yang, Z. Wang, and X. Liu. 360 deg full-parallax light-field display using panoramic camera. *Appl. Opt.*, 55(17):4729–4735, 2016. doi: 10.1364/AO.55.004729

[43] Y. Takaki and S. Uchida. Table screen 360-degree three-dimensional display using a small array of high-speed projectors. *Opt. Express*, 20(8):8848–8861, 2012. doi: 10.1364/OE.20.008848

[44] F. Tian, H. Wang, Y. Fang, H. Pan, and X. Xia. A swept volume display system using a planetary gear structure based on parallel moving. *Journal of Display Technology*, 8(8):457–463, 2012. doi: 10.1109/JDT.2012.2196790

[45] R. A. Ulichney. Void-and-cluster method for dither array generation. In *Human Vision, Visual Processing, and Digital Display IV*, vol. 1913, pp. 332 – 343. International Society for Optics and Photonics, 1993. doi: 10.1117/12.152707

[46] L. Wang, S. Tabata, H. Xu, Y. Hu, Y. Watanabe, and M. Ishikawa. Dynamic depth-of-field projection mapping method based on a variable focus lens and visual feedback. *Opt. Express*, 31(3):3945–3953, 2023. doi: 10.1364/OE.478416

[47] Z. Wang, A. Bovik, H. Sheikh, and E. Simoncelli. Image quality assessment: from error visibility to structural similarity. *IEEE Transactions on Image Processing*, 13(4):600–612, 2004. doi: 10.1109/TIP.2003.819861

[48] Y. Watanabe and M. Ishikawa. High-speed and high-brightness color single-chip DLP projector using high-power LED-based light sources. In *26th International Display Workshops, IDW 2019*, pp. 1350–1352, 2019. doi: 10.36463/IDW.2019.1350

[49] Y. Watanabe, G. Narita, S. Tatsuno, T. Yuasa, K. Sumino, and M. Ishikawa. High-speed 8-bit image projector at 1,000 fps with 3 ms delay. In *22nd International Display Workshops, IDW 2015*, pp. 1064–1065, 2015.

[50] X. Xia, X. Liu, H. Li, Z. Zheng, H. Wang, Y. Peng, and W. Shen. A 360-degree floating 3D display based on light field regeneration. *Opt. Express*, 21(9):11237–11247, 2013. doi: 10.1364/OE.21.011237

[51] H. Xu, L. Wang, S. Tabata, Y. Watanabe, and M. Ishikawa. Extended depth-of-field projection method using a high-speed projector with a synchronized oscillating variable-focus lens. *Appl. Opt.*, 60(13):3917–3924, 2021. doi: 10.1364/AO.419470

[52] G. Ye, A. State, and H. Fuchs. A practical multi-viewer tabletop autostereoscopic display. In *2010 IEEE International Symposium on Mixed and Augmented Reality (ISMAR)*, pp. 147–156, 2010. doi: 10.1109/ISMAR.2010.5643563

[53] S. Zhang. High-speed 3D shape measurement with structured light methods: A review. *Optics and Lasers in Engineering*, 106:119–131, 2018. doi: 10.1016/j.optlaseng.2018.02.017